Influence of cerium content on the corrosion behavior of Al-Co-Ce amorphous alloys in 0.6 M NaCl solution

L.M. Zhang[a,b], S.D. Zhang[c], A.L. Ma[a], A.J. Umoh[a,b], H.X. Hu[a], Y.G. Zheng[a,*], B.J. Yang[c], J.Q. Wang[c,*]

[a] CAS Key Laboratory of Nuclear Materials and Safety Assessment, Institute of Metal Research, Chinese Academy of Sciences, 62 Wencui Road, Shenyang 110016, PR China

[b] School of Materials Science and Engineering, University of Science and Technology of China, 72 Wenhua Road, Shenyang 110016, PR China

[c] Shenyang National Laboratory for Materials Science, Institute of Metal Research, Chinese Academy of Sciences, 72 Wenhua Road, Shenyang 110016, PR China

A B S T R A C T

The effect of cerium content on the corrosion behavior of Al-Co-Ce amorphous alloys in 0.6 M NaCl solution was investigated by cyclic polarization, Mott-Schottky and X-ray photoelectron spectroscopy techniques. Results indicated that the open circuit potential of Al-Co-Ce amorphous alloys displayed a decreased tendency with the increase in Ce content, and the amorphous alloy with 4 at.% Ce presented both the lowest passive current density and donor density indicating the best corrosion resistance, while adding excess Ce led to the reduced corrosion resistance of Al-Co-Ce alloys. Furthermore, it was found that a low Ce content is beneficial to the formation of a more protective passive film on Al-Co-Ce amorphous alloys, and the corrosion inhibition reactions of Al-Co-Ce alloys in 0.6 M NaCl solution were changed with the increase in Ce content and the detailed reasons were discussed.

1. Introduction

Al-based metallic glasses, also called Al-based amorphous alloys, were discovered for the first time in the United States and Japan concurrently in 1988 [1,2]. Since then, both scientific and technological interests in these materials have been generated due to their unique properties, e.g., high strength to weight ratio, superior wear and corrosion resistance and flexible alloy composition, which often surpass those of conventional structural materials displaying the potential application in the fields of automotive, marine and aviation industries [3–5].

With the development of Al-based amorphous alloys, Al-TM-RE (TM: Transition Metal; RE: Rare Earth) as an important composition system has been extensively investigated because of good glass forming ability (GFA) and superior corrosion resistance, such as Al-Ni-Y [5], Al-Ni-Ce [3,6] and Al-Co-Ce [7]. Among them, Al-Co-Ce amorphous alloys show a series of prominent properties, e.g., good thermal stability, wide composition scope with amorphous structure and tunable property based on Co and Ce [6–9]. In corrosion protection, Al-Co-Ce amorphous alloys can serve as a barrier preventing the invasion of Cl^- ions, serve as a sacrificial anode and also release corrosion-inhibition ions on demand based on different pH values [7,9,10]. Thus, they are particularly suitable as multifunctional coatings to protect aluminum alloys from corrosion. Relevant investigations have shown that the protectiveness abilities displayed by these alloys are superior to the conventional Al-clad coatings in terms of both polarization and maximum scratch size protected on AA2024-T3 [6,8,9,11–17]. Nevertheless, the composition range with good corrosion resistance presented in relevant studies is a little wide (Co: 6$\tilde{8}$ at.%; Ce: 3$\tilde{5}$ at.%). Therefore, it is worth further optimizing the composition of Al-Co-Ce amorphous alloys with better corrosion resistance to substitute the Al-clad coatings.

In order to achieve the aforementioned goal, one primary task is to understand the roles of the elements in Al-Co-Ce amorphous alloys, since it is generally considered that the corrosion resistance of an alloy essentially depends on its composition [6–9,18–20]. For a specific environment with constant pH and concentration of Cl^- ions, the different corrosion performances of Al-Co-Ce alloys can be obtained through changing the contents of Co and Ce. For instance, the Al-Co-Ce amorphous alloys with a low Co content (3$\tilde{5}$ at.%) and a low Ce content of (3$\tilde{5}$ at.%) have a moderately low open circuit

* Corresponding authors.
E-mail addresses: ygzheng@imr.ac.cn (Y.G. Zheng), jqwang@imr.ac.cn (J.Q. Wang).

potential (OCP) and can avoid the cathodic over-protection at the same time. However, when choosing a high Co content (6δ at.%) and a low Ce content (3δ at.%), the highest resistance to localized corrosion can be obtained [6]. Therefore, the contents of Co and Ce play important roles in corrosion performances of Al-Co-Ce amorphous alloys, and it is important to understand the roles of the two elements before designing the composition of the alloy.

The presence of Co can increase the rate of oxygen reduction or hydrogen evolution reaction leading to the increased OCP [6,8,14,21]. Meanwhile, Co usually has a lower dissolution rate than Al and Ce, and the ionic product (Co^{2+}) can reduce the rate of anodic dissolution and inhibit the localized corrosion [8,14]. The existence of the rare-earth element Ce can improve the GFA of Al-Co-Ce amorphous alloys. In terms of corrosion protection, Ce^{3+} also has a good property of corrosion inhibition. The corrosion inhibition mechanism of Ce^{3+} is attributed to the enriched oxides or hydroxides of Ce formed on the cathodic surface, which hinder the oxygen reduction reaction [22–24]. However, the Ce^{3+} species used in the above-mentioned work are all corrosion inhibitors such as $Ce(NO_3)_3$ and $CeCl_3$ [25–30]. To improve the corrosion resistance of alloys and the flexibility of Ce in use, researchers also try to add Ce into some alloys. While the content of Ce in these alloys is usually low because of the limited solid solubility, which leads to a weak corrosion inhibition effect. In addition, adding Ce into some composite coatings has also been reported, and the relevant results indicate that there exists an optimal Ce concentration, below or above which will lead to an increase in corrosion rate [30,31]. The decrease in corrosion resistance can be related to some defects formed in the film. The investigations of Ce content on the corrosion resistance of Al-based amorphous alloys are numbered, among which some pioneering investigations on the role of Ce in Al-Co-Ce amorphous alloys have been made [6,8,21]. However, the Ce content with the best corrosion resistance in Al-Co-Ce amorphous alloys is still undefined. Moreover, the questions of what is the influence of Ce content on the corrosion behavior of Al-Co-Ce amorphous alloys and how does Ce content affect the electrochemical corrosion behavior are both vague and unanswered.

Herein, five kinds of amorphous alloys of $Al_{93-x}Co_7Ce_x$ (x = 3, 4, 5, 6 and 7) were prepared respectively. The selection of this composition range is due to its superior corrosion resistance and GFA based on previous studies [6,15]. The effect of Ce content on the corrosion behavior of Al-Co-Ce amorphous alloys was studied by means of cyclic polarization, Mott-Schottky and XPS techniques. And the influences of Ce content on the OCP, the semiconductor properties of passive film, and the corrosion inhibition mechanism of Al-Co-Ce amorphous alloys were also discussed in details. The aim of this work is to deepen the horizon in understanding the role of Ce in the corrosion behavior of Al-Co-Ce amorphous alloys and to find out the optimal Ce content with the best corrosion resistance for Al-Co-Ce amorphous alloys.

2. Experimental

2.1. Materials and samples preparation

Al-Co-Ce master alloy ingots with the nominal compositions of $Al_{90}Co_7Ce_3$, $Al_{89}Co_7Ce_4$, $Al_{88}Co_7Ce_5$, $Al_{87}Co_7Ce_6$ and $Al_{86}Co_7Ce_7$ (surrounded by red dashed line in Fig. 1) were prepared by melting appropriate amounts of pure metals: Al (99.999%), Co (99.995%) and Ce (99.9%). Melting at least four times was conducted in an arc furnace under the highly pure argon atmosphere to ensure compositional homogeneity. The Al-Co-Ce amorphous ribbons were fabricated by induction melting the master alloys ingot in a silica crucible under the protection of argon, and then ejecting it onto a copper wheel rotating at a speed of 35 m/s using a melt spinner

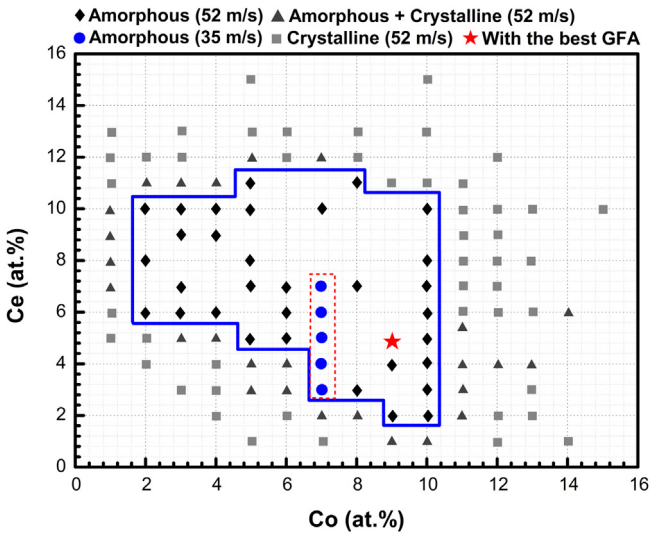

Fig. 1. The composition-structure map [7,14] of Al-Co-Ce based on at.% Co and at.% Ce present in solid solution Al (the selected composition region in this paper was surrounded by red dashed line and red star denotes the composition with the best GFA based on cluster stability lines model).

(D-7400, Edmund Bühler, Hechingen, Germany). The thickness and width of all ribbons are about 30 μm and 3.5 mm, respectively. The ribbons for electrochemical tests were cut into pieces with a length of 10 mm firstly, then were connected with the conducting copper wires, and finally were sealed with epoxy resin in a vacuum drying oven to ensure no bubbles on the samples. The exposed area (cross section) of the electrochemical samples is about 10^{-3} cm^2 and the accurate value can be tested by a confocal laser scanning microscope (OLS4000, Olympus, Tokyo, Japan).

2.2. Microstructure characterization

The X-ray diffraction (XRD, D/Max 2400, Rigaku, Tokyo, Japan) with monochromatic Cu Kα radiation (λ = 0.1542 nm) was used to characterize the amorphicity of the melt-quenched ribbons. A transmission electron microscope (TEM, JEOL-2100, JEOL Ltd., Tokyo, Japan) was used to further identify whether the ribbons contained nanocrystals. The samples for TEM observation were prepared by ion beam thinning with liquid nitrogen cooling. The corrosion morphology and chemical composition of the ribbons were revealed with the help of the scanning electron microscopy equipped with an energy dispersive X-ray detector (SEM/EDS, INSPECT F50, FEI, Hillsboro, USA).

2.3. Electrochemical tests

The electrochemical tests of five kinds of amorphous alloys were conducted in 0.6 M NaCl solution (pH 6.5) by an electrochemical workstation (Interface 1000, Gamry Inc., USA). A traditional three-electrode cell (i.e., a platinum plate as the counter electrode, a saturated calomel electrode (SCE) as the reference electrode and the sample as the working electrode) was used for all electrochemical tests. The cross section with an area of 10^{-3} cm^2 was selected as the test surface. Prior to the electrochemical measurements, the cross sections were ground with 400, 1000 and 2000 grit SiC sandpapers in sequence, and then were polished using 1 μm diameter diamond polishing paste. The cyclic polarization tests were carried out at 0.5 mV/s starting from −10 mV vs. OCP and the reverse scan was executed when the potential reached 0 V vs. SCE or the current density achieved 10^{-4} A/cm^2. In order to evaluate the semiconductor properties of the passive films of Al-Co-Ce amorphous

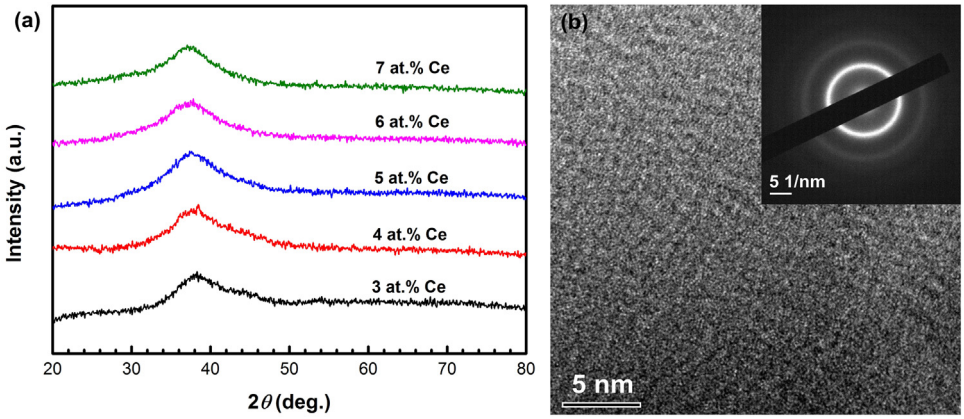

Fig. 2. (a) XRD patterns of $Al_{93-x}Co_7Ce_x$ (x = 3, 4, 5, 6, 7) melt-spun ribbons prepared with 35 m/s circumferential wheel speed, (b) the bright-field TEM image and the selected area electronic diffraction pattern (SEAD, inset) of the $Al_{90}Co_7Ce_3$ melt-spun ribbon.

Table 1
Nominal composition and the actual composition of $Al_{93-x}Co_7Ce_x$ (x = 3, 4, 5, 6, 7) melt-spun ribbons.

Nominal composition(at.%)	$Al_{90}Co_7Ce_3$	$Al_{89}Co_7Ce_4$	$Al_{88}Co_7Ce_5$	$Al_{87}Co_7Ce_6$	$Al_{86}Co_7Ce_7$
Actual composition(at.%)	$Al_{90.01}Co_{6.91}Ce_{3.08}$	$Al_{88.73}Co_{7.19}Ce_{4.08}$	$Al_{87.51}Co_{7.26}Ce_{5.23}$	$Al_{87.22}Co_{6.81}Ce_{5.97}$	$Al_{85.90}Co_{7.08}Ce_{7.02}$

alloys, Mott-Schottky plots were measured at a scanning rate of 20 mV/s. To guarantee the reliability of the results, the electrochemical measurements were repeated 6 times and the results that could represent the mean value were selected. In addition, the statistical method was also used for the analysis of some electrochemical data considering the volatility of data.

2.4. XPS characterization

The surface composition of the Al-Co-Ce amorphous alloys with different Ce contents was characterized by a X-ray photoelectron spectrometer (XPS, ESCALAB250, Waltham, USA) with Al Kα excitation ($h\nu$ = 1486.6 eV). The samples for XPS characterization were immersed in 0.6 M NaCl solution for four hours and four days, respectively. The wheel side instead of cross section was selected as the test surface considering the small exposed area (10^{-3} cm^2) of cross section which was difficult for XPS test. The position of the adventitious carbon component (284.6 eV) was used for the calibration of binding energy. The standard binding energy of Al 2p, Co $2p_{3/2}$ and Ce $3d_{5/2}$ core levels was based on the NIST XPS database. The depth profiles were characterized by in situ XPS ion beam sputtering with 3 kV, 2 mA argon ions at a sputtering rate of 0.1 nm/s. The software of XPSPEAK 4.1 was used for the XPS data processing.

3. Results and discussion

3.1. Microstructure and composition characterization

The XRD patterns of five kinds of Al-Co-Ce alloys are shown in Fig. 2a. There only exists one broad hump at the angle of 2θ = 38° for each alloy indicating the amorphous structure. In order to identify whether the alloys contain nanocrystals, the alloy with 3 at.% Ce which has a low GFA due to its proximity to amorphous-nanocrystals composition (Fig. 1) is analyzed using selected area electron diffraction (SAED). The corresponding SAED pattern (Fig. 2b) displays diffuse halo rings confirming the fully amorphous structure. Furthermore, the actual compositions of five kinds of amorphous ribbons are shown in Table 1. It is obvious that there are only unsubstantial differences between the nominal composition and the actual composition for each Al-Co-Ce amorphous alloy. Therefore, the amorphous alloys prepared in this research are reliable.

3.2. Open circuit potentials

Fig. 3a shows the OCP curves of five kinds of Al-Co-Ce amorphous alloys in 0.6 M NaCl solution. Each sample attains a stable OCP after 2000 s' immersion, and the stable OCP displays a decreased tendency with the increase in Ce content. Furthermore, the statistical results of OCP derived from six parallel samples are exhibited in Fig. 3b. It is obvious that there exists a linear relationship between the stable OCP and the Ce content, and the linear equation is as follows:

$$y_{OCP} = -0.015x_{Ce} - 0.573 \quad (1)$$

where y_{OCP} represents the value of the stable OCP (V vs. SCE) and x_{Ce} represents Ce content (at.%). With the help of this equation, the stable OCP of Al-Co-Ce amorphous alloys with 7 at.% Co and different Ce contents can be predicted to some degree.

3.3. Cyclic polarization behavior of Al-Co-Ce amorphous alloys

The cyclic polarization curves of Al-Co-Ce amorphous alloys with different Ce contents are presented in Fig. 4. Clearly, the alloys with 3 at.% Ce and 4 at.% Ce have a low passive current density with an order of magnitude of 10^{-6} A/cm^2. At the same time, the hysteresis loop whose size reflects the resistance to pitting varies obviously with different Ce contents. The alloys with a low Ce content (3̃5 at.%) have the small hysteresis loops. However, the hysteresis loops become big when Ce contents are increased to 6 at.% and 7 at.%, indicating the decreased resistance to pitting. Fig. 5 shows the statistical results of passive current density (i_{pass}), pitting potential (E_{pit}), repassivation potential (E_{rp}) and corrosion potential (E_{corr}) for Al-Co-Ce alloys with different Ce contents, and these results are based on the six repeated tests for each alloy. It is obvious that the i_{pass} decreases slightly at first and then gradually increases with the increase in Ce content (Fig. 5a). And the alloy with 4 at.% Ce presents the lowest i_{pass} indicating the best corrosion resistance, while the alloy with 7 at.% Ce has the highest i_{pass} implying the worst corrosion resistance. For the E_{pit}, it generally displays a decreased tendency with the increase in Ce content except the alloys with

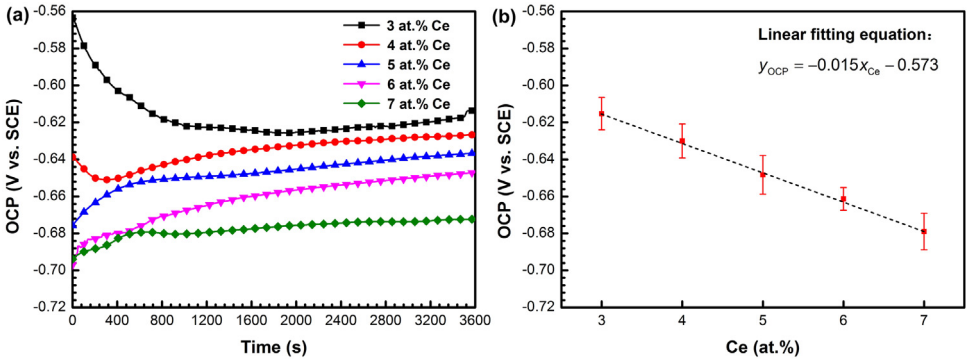

Fig. 3. (a) The OCP curves of $Al_{93-x}Co_7Ce_x$ ($x = 3, 4, 5, 6, 7$) amorphous alloys in 0.6 M NaCl solution for 3600 s, (b) the statistical results of stable OCP derived from six repeated tests for $Al_{93-x}Co_7Ce_x$ ($x = 3, 4, 5, 6, 7$) amorphous alloys.

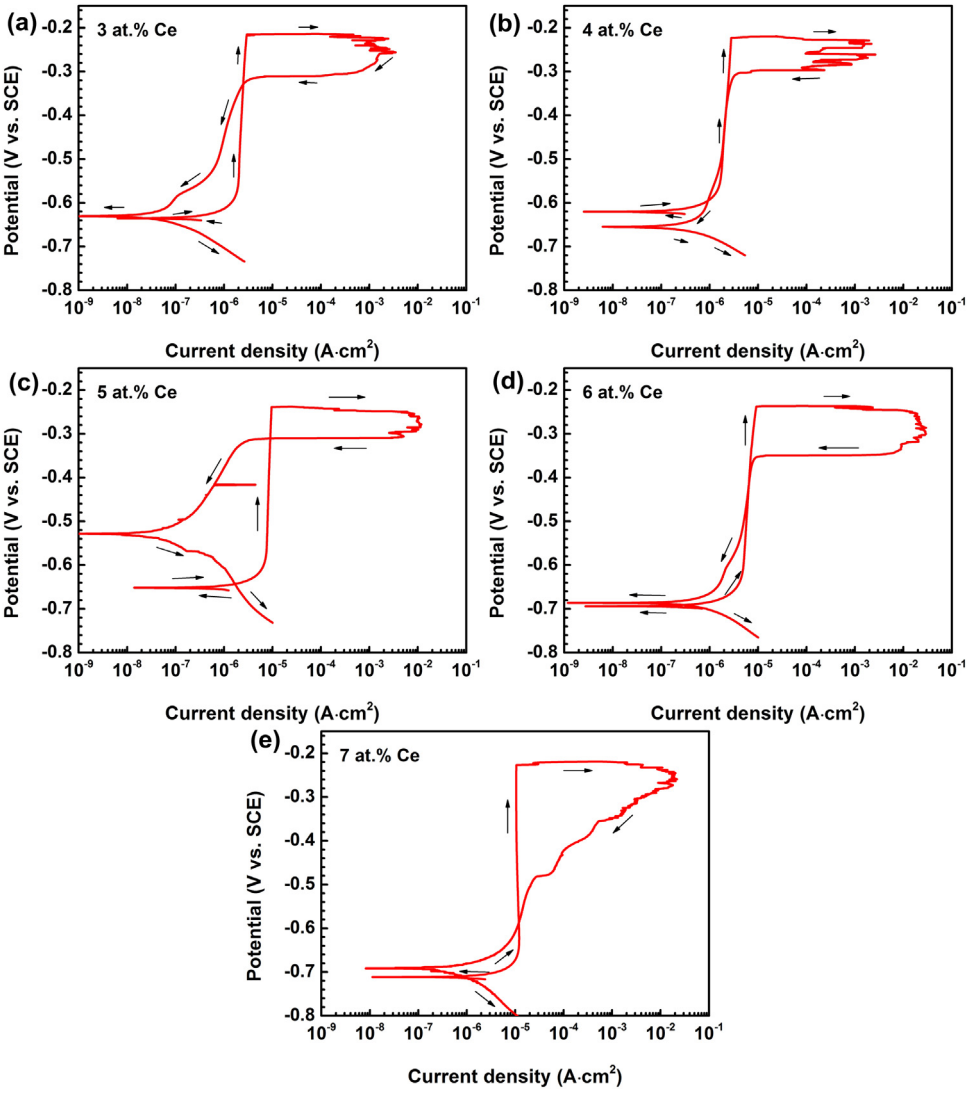

Fig. 4. Cyclic polarization curves of $Al_{93-x}Co_7Ce_x$ ($x = 3, 4, 5, 6, 7$) amorphous alloys in 0.6 M NaCl solution (the arrows indicating the scanning direction).

low Ce contents (3 at.% and 4 at.%) which have the similar E_{pit}. For the E_{rp}, there also displays a declined trend with the increase in Ce content, indicating the decreased repassivation ability with the increased Ce content. Concerning the E_{corr}, a similar linear relationship between the potential and Ce content compared with the OCP is displayed, which supports the aforementioned analysis of OCP.

3.4. Semiconductor properties of passive films

Semiconductor properties of the passive film of aluminum or aluminum alloys have been widely reported [32–37], and the relevant results indicate that the passive film of aluminum or aluminum alloys presents either *n*-type [32,34–36] or *p*-type property [33] depending on the environmental conditions. In order to reveal the

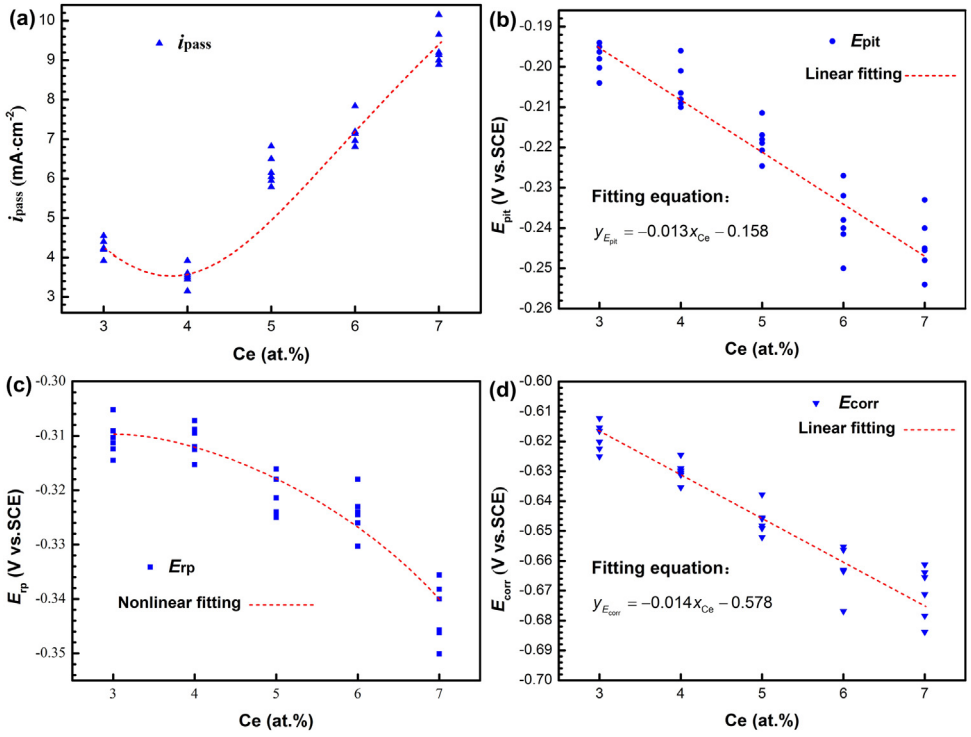

Fig. 5. Statistical results of i_{pass}, E_{pit}, E_{rp}, E_{corr} derived from six repeated tests of cyclic polarization curves of $Al_{93-x}Co_7Ce_x$ (x = 3, 4, 5, 6, 7) amorphous alloys.

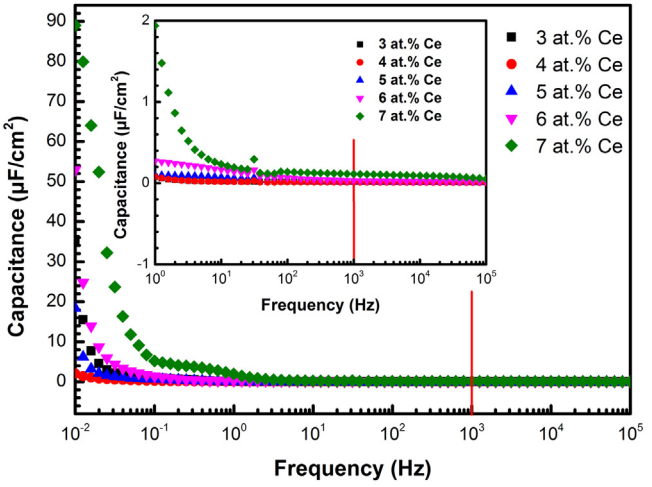

Fig. 6. Capacitance plots of $Al_{93-x}Co_7Ce_x$ (x = 3, 4, 5, 6, 7) amorphous alloys with the change of frequency in 0.6 M NaCl solution.

effect of Ce content on the semiconductor properties of passive film, the Mott-Schottky curves are measured. It is noteworthy that the results of Mott-Schottky tests are sensitive to frequency, so the frequency selected should be located in the range where the electrode capacitance is stable. Fig. 6 displays the capacitance plots with the change of frequency. Obviously, the capacitance is independent of frequency in the range from 100 Hz to 100 kHz. Thus, an included frequency of 1000 Hz is selected in this work to eliminate the capacitance dependence on frequency. Fig. 7a shows the Mott-Schottky plots of five kinds of amorphous alloys and all plots exhibit the positive linear zone from −0.75 V to −0.2 V vs. SCE which is almost the range from the OCP to E_{pit}, indicating that the passive films of Al-Co-Ce amorphous alloys formed in 0.6 M NaCl solution all have the properties of n-type semiconductor. According to the Mott-Schottky equation of n-type semiconductor:

$$C^{-2} = \frac{2}{\varepsilon_r \varepsilon_0 e N_D}\left(E - E_{FB} - \frac{kT}{e}\right) \quad (2)$$

where ε_r is the relative dielectric constant of Al oxide, taken as 10 based on relevant investigation [34], ε_0 is the vacuum permittivity (8.85×10^{-14} F·cm^{-1}), N_D is the donor density in an n-type passive film, E is the applied potential (V vs. SCE), E_{FB} is the flat band potential (V vs. SCE), k is Boltzmann constant (1.38×10^{-23} J·K^{-1}), e is electron charge (1.6×10^{-19} C), and T is absolute temperature (K). N_D can be obtained based on the slope (K_{slope}) of Eq. (2) and the expression of N_D is as follows:

$$K_{slope} = \frac{dC^{-2}}{dE} = \frac{2}{\varepsilon_r \varepsilon_0 e N_D} \quad (3)$$

$$N_D = \frac{2}{\varepsilon_r \varepsilon_0 e}\left(\frac{dC^{-2}}{dE}\right)^{-1} \quad (4)$$

Fig. 7b presents the plots of N_D with different Ce contents. The order of magnitude of N_D for all Al-Co-Ce alloys is about 10^{21} cm^{-3}, which is close to the value of 2024 aluminum alloy in borate buffer solution [37] and less than that of 3003 aluminum alloy in sodium sulphate solution [34]. At the same time, the values of N_D are close to that of Fe-Cr alloy and stainless steel in the buffer solution (10^{20} ~10^{22} cm^{-3}) [38], indicating the good protection of the passive films of Al-Co-Ce amorphous alloys. More precisely, the alloy with 4 at.% Ce has the lowest N_D of 1.63×10^{21}/cm^3, and N_D presents an increased trend with the increase in Ce content and the alloy with 7 at.% Ce has the highest N_D of 6.34×10^{21}/cm^3. Generally, N_D reflects the conductivity of passive film, and a lower N_D means a higher resistance of the passive film indicating the good shield of passive film. Wang et al. also discovered that a good corrosion resistance of Fe-based amorphous alloys corresponds to a low N_D of the passive film [39]. Therefore, it can be inferred that the alloy with 4 at.% Ce has the best corrosion resistance while the alloy with 7 at.% Ce

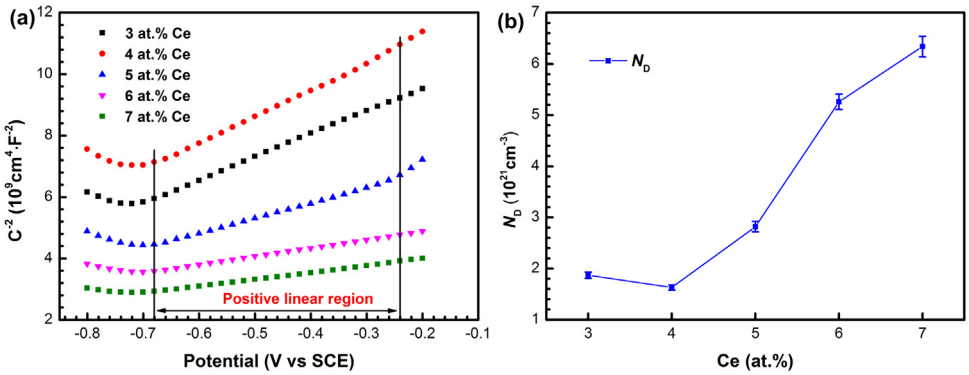

Fig. 7. (a) Mott-Schottky plots of five kinds of Al-Co-Ce amorphous alloys in 0.6 M NaCl solution, (b) donor densities of passive films of $Al_{93-x}Co_7Ce_x$ (x = 3, 4, 5, 6, 7) amorphous alloys.

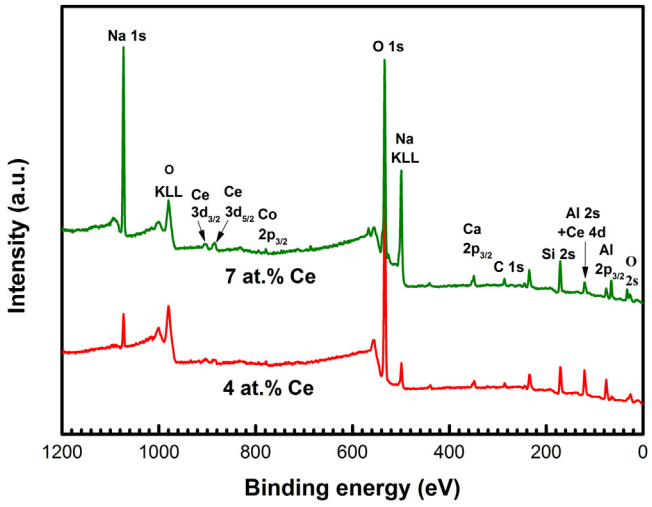

Fig. 8. XPS full spectra of the passive films of $Al_{89}Co_7Ce_4$ and $Al_{86}Co_7Ce_7$ amorphous alloys after immersion in 0.6 M NaCl for four days.

presents the worst corrosion resistance based on the analysis of N_D, which is consistent with the results of cyclic polarization.

3.5. *Chemical analysis and corrosion morphology of the passive films*

To provide an indepth information about the composition of the passive films of Al-Co-Ce amorphous alloys, the XPS technology is adopted to characterize the alloys with 4 at.% Ce and 7 at.% Ce which are immersed in 0.6 M NaCl solution for four days. Fig. 8 shows the XPS spectra of the alloys with 4 at.% Ce and 7 at.% Ce, and there exist obvious peaks of Ce 3d, Co 2p, Al 2p for both alloys. Furthermore, the detailed XPS spectra of Al 2p, Co $2p_{3/2}$ and Ce $3d_{5/2}$ of the alloys with 4 at.% Ce and 7 at.% Ce are exhibited in Figs. 9 and 10. For the alloy with 4 at.% Ce (Fig. 9), the spectrum of Al 2p contains three components of metallic state aluminum (Al (0)), aluminum oxide (Al_2O_3) and aluminum hydroxide ($Al(OH)_3$), and their relative contents are 29.9%, 30.9% and 39.2% respectively. The peak positions of the three components are 72.90 eV, 73.97 eV and 75.98 eV, respectively. Similarly, the alloy with 7 at.% Ce (Fig. 10) also has the same components in the film, while the relative contents are 25.2%, 18.6% and 56.2% corresponding to Al (0), Al_2O_3 and $Al(OH)_3$ respectively. Apparently, the alloy with 7 at.% Ce has less Al_2O_3 but more $Al(OH)_3$ than the former. Note that, the Al_2O_3 film is compact and usually exhibits the superior protectiveness while the $Al(OH)_3$ film is loose and usually has the weak protectiveness. Meanwhile, the main components of the passive film for Al-Co-Ce amorphous alloy are the oxide and hydroxide of aluminum due to the extremely high content of aluminum in the matrix and its high affinity for oxygen. Thus, it can be deduced that the alloy with a low Ce content has a more protective film than the one with a high Ce content, which gives a good explanation for the difference in corrosion resistance of Al-Co-Ce amorphous alloys with different Ce contents. For the spectrum of Co $2p_{3/2}$, both the above-mentioned alloys just display the metallic state Co (0) corresponding to 778.2 eV. The spectrum of Ce $3d_{5/2}$ of the alloy with 4 at.% Ce indicates that there exist Ce (0) and Ce_2O_3 in the film, and their relative contents are 38.3% and 61.7 respectively. While for the alloy with 7 at.% Ce, the spectrum of Ce $3d_{5/2}$ shows that there is CeO_2 besides Ce (0) and Ce_2O_3 and the relative content of CeO_2 is as much as 23.6 at.%. The existence of CeO_2 seems to imply some changes in corrosion inhibition reactions for Al-Co-Ce amorphous alloys with the increase in Ce content.

Fig. 11a and b shows the concentration depth profiles of Al, Co, Ce, O and Cl in the passive films of the alloys with 4 at.% Ce and 7 at.% Ce respectively, both the alloys are immersed in 0.6 M NaCl solution for four hours. The thicknesses of the passive films are about 9 nm and 12 nm for the alloys with 4 at.% and 7 at.% Ce, respectively. Notably, the contents of Cl^- in both passive films are very low. For convenience, the effect of Cl^- on the corrosion performance is ignored. As regards to the alloy with 7 at.% Ce, there exhibits a higher oxygen content in both the surface of passive film and the interface between passive film and substrate compared with the alloy with 4 at.% Ce. Furthermore, the difference of the oxygen content in both films is more evident when the two alloys are immersed in 0.6 M NaCl for four days (Fig. 11c and d), and the thicknesses of the surface films for the alloys with 4 at.% Ce and 7 at.% Ce are about 30 nm and 54 nm, respectively. It is noteworthy that the oxygen content has an important impact on the dissolution processes of Ce [22]. Therefore, the effect of Ce content on the corrosion resistance of Al-Co-Ce amorphous alloys can also be related to the oxygen content in the film, and the relevant discussion is shown in Section 3.7.

The corrosion morphologies of Al-Co-Ce amorphous alloys (cross sections) with 4 at.% Ce and 7 at.% Ce are shown in Fig. 12. After immersion in 0.6 M NaCl solution for four days, the uniform surface film is formed on the alloy with 4 at.% Ce, and there is no obvious localized corrosion (Fig. 12a and b). For the alloy with 7 at.% Ce, there displays apparent corrosion cracks on the surface film (Fig. 12c and d) indicating the poor corrosion resistance. The results of corrosion morphologies corroborate the electrochemical results above.

3.6. *Effect of Ce content on the OCP of Al-Co-Ce amorphous alloys*

The stable OCP of Al-Co-Ce amorphous alloys displays a decreased trend with the increase in Ce content (Fig. 3). As the

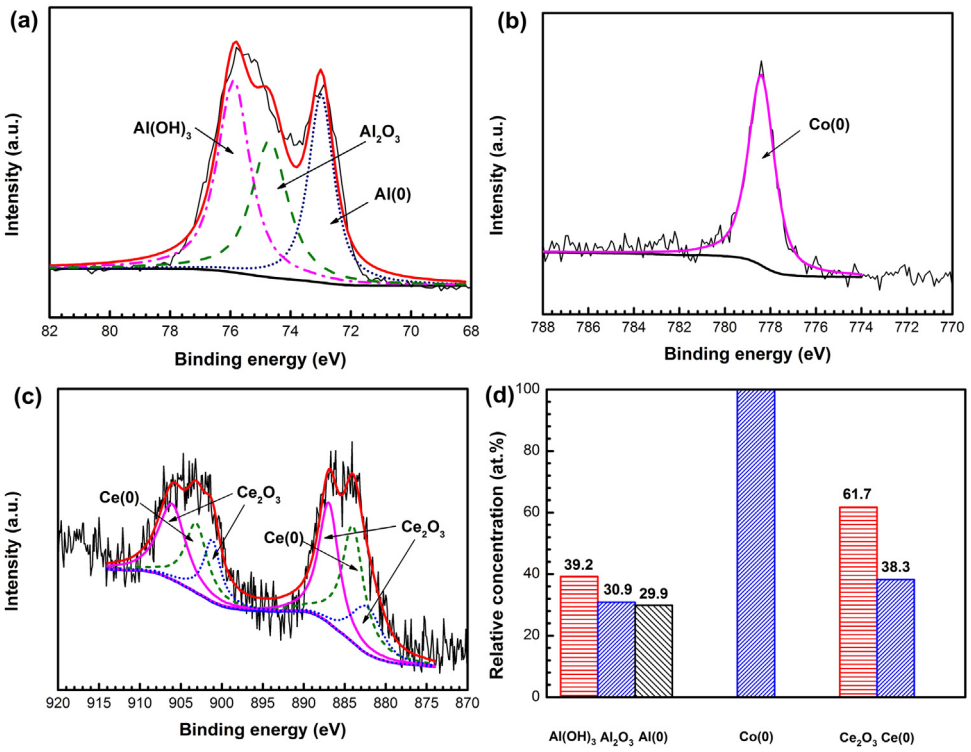

Fig. 9. XPS spectra of (a) Al 2p, (b) Co $2p_{3/2}$, (c) Ce $3d_{5/2}$ for the passive films of $Al_{89}Co_7Ce_4$ amorphous alloy after immersion in 0.6 M NaCl for four days, (d) the relative content of each substance.

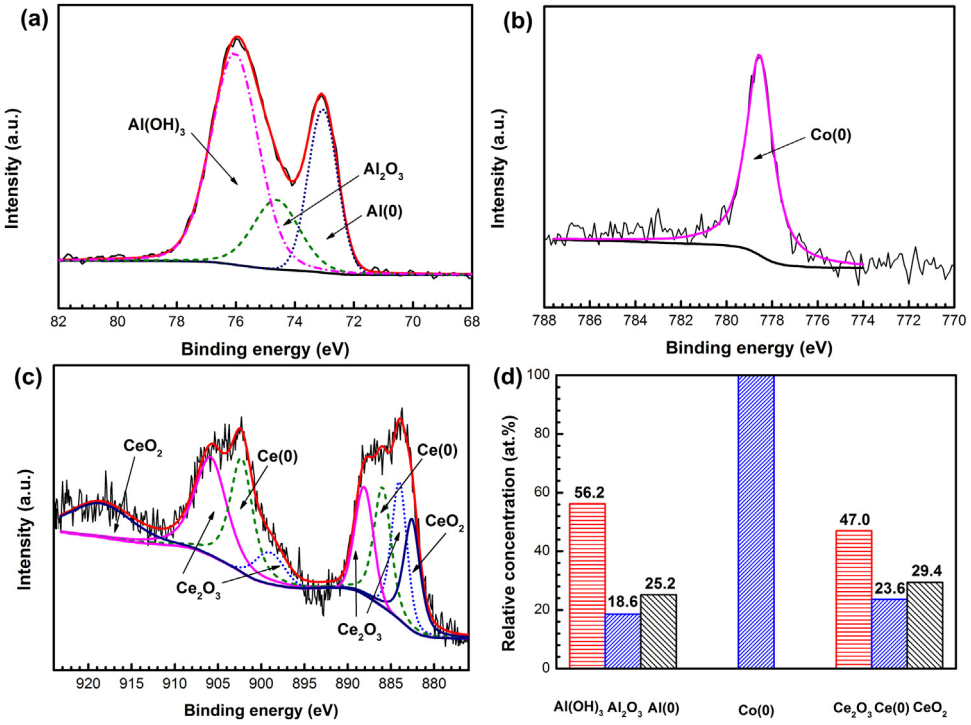

Fig. 10. XPS spectra of (a) Al 2p, (b) Co $2p_{3/2}$, (c) Ce $3d_{5/2}$ for the passive films of $Al_{86}Co_7Ce_7$ amorphous alloy after immersion in 0.6 M NaCl for four days, (d) the relative content of each substance.

OCP is the coupling potential of cathodic reaction and anodic reaction, the change of OCP is closely related to the cathodic and anodic reactions on working electrode. With respect to the anodic reaction of Al-Co-Ce amorphous alloys, there exhibits an increased i_{pass} with the increase in Ce content on the whole, which means that Ce promotes the anodic reaction. As we know, the activity of Ce is higher than Al and Co, and Ce^{3+} also has a higher migration rate than Al^{3+} [24], so the anodic reaction will be accelerated with the increase in Ce content. For the cathodic reaction, the corrosion inhibition effect of Ce^{3+} on cathodic reaction has been widely

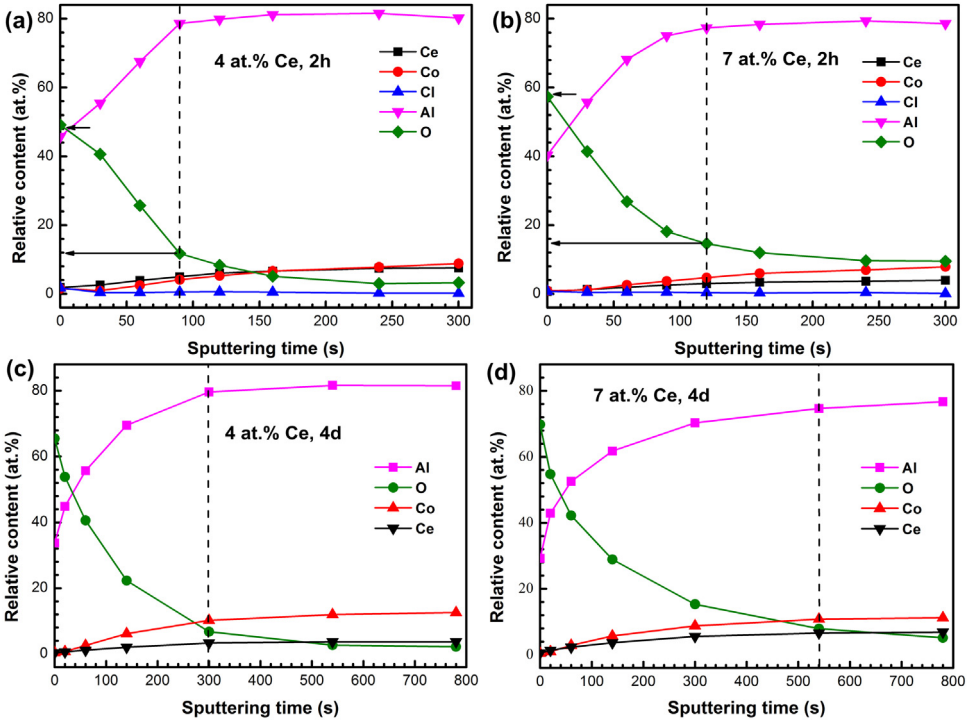

Fig. 11. Depth profiles of Al, Co, Ce, O and Cl in the passive films formed on (a) $Al_{89}Co_7Ce_4$ and (b) $Al_{86}Co_7Ce_7$ amorphous alloys after immersion in 0.6 M NaCl solution for four hours. (c) and (d) are the depth profiles of Al, Co, Ce, O in the passive films formed on $Al_{89}Co_7Ce_4$ and $Al_{86}Co_7Ce_7$ amorphous alloys after immersion in 0.6 M NaCl for four days, respectively.

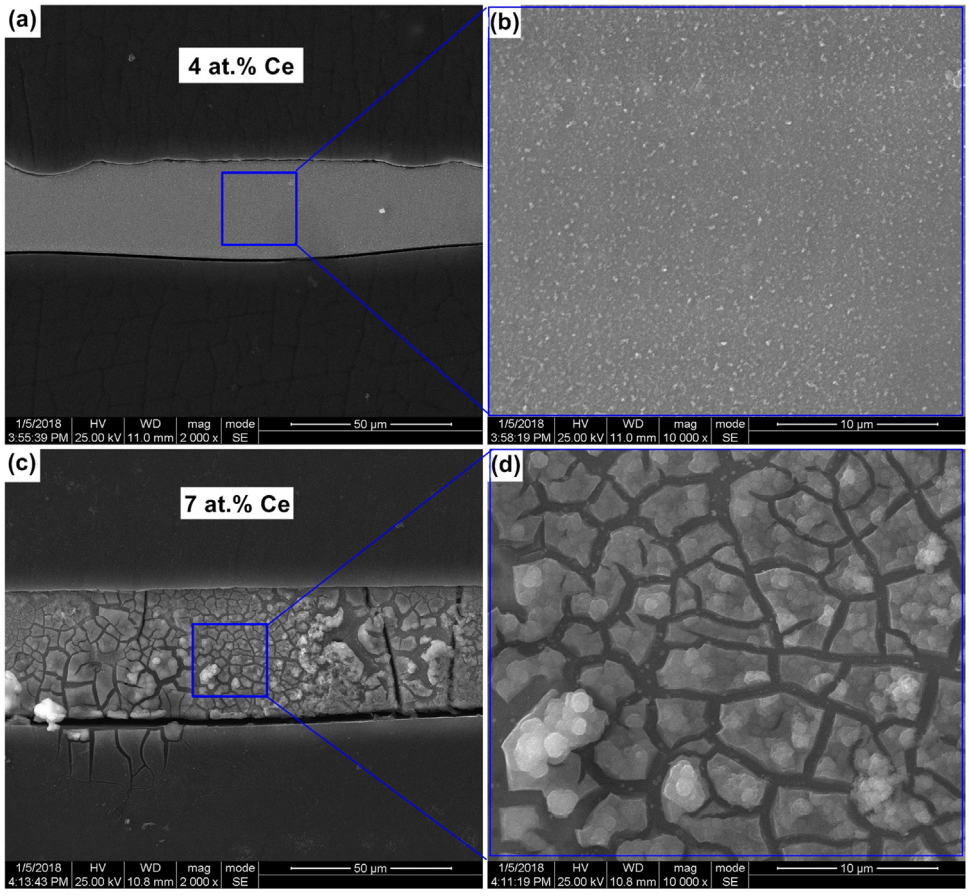

Fig. 12. Corrosion morphologies (cross sections) of (a) $Al_{89}Co_7Ce_4$ and (b) $Al_{86}Co_7Ce_7$ amorphous alloys after immersion in 0.6 M NaCl solution for four days.

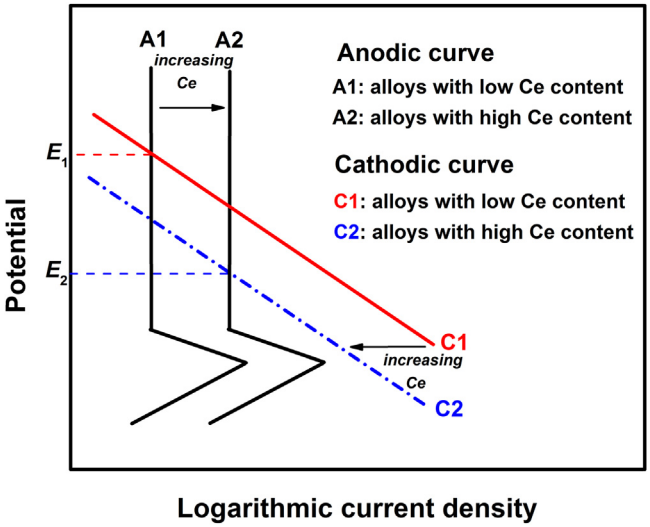

Fig. 13. The impact schematic of Ce content on OCP of Al-Co-Ce amorphous alloys in 0.6 M NaCl solution.

reported [21,22,24,40,41]. The mechanism of corrosion inhibition of Ce^{3+} is attributed to the formation of Ce oxides or hydroxides on the surface of cathode, which hinder the oxygen reduction reaction [22–24]. However, Ce^{3+} cannot play a significant role in corrosion inhibition unless it achieves or exceeds a certain concentration which is also called the critical concentration of Ce ions ($C_{crit,Ce}$). According to equation of $C_{crit,Ce}$ [8]:

$$\log C_{crit,Ce} = -2.4 + 0.8 \times \log C_{Cl^-} \quad R^2 = 0.94 \tag{5}$$

where $C_{Cl}{}^-$ is the concentration of Cl^- in the solution, R^2 is the relative calculation accuracy. The $C_{crit,Ce}$ in 0.6 M NaCl solution can be calculated out and this value is about 2.8 mM. Assuming that the dissolution rate of Ce is same for different samples, it will take different times to reach the $C_{crit,Ce}$ due to the different Ce contents. Usually, the higher Ce content, the shorter time to reach the $C_{crit,Ce}$ and the larger accumulation of cerium-containing precipitations on the surface of cathode, both of which contribute to enhancing inhibition effect on the cathodic reaction. Nonetheless, it will take a long time to reach the $C_{crit,Ce}$ for the whole surface of Al-Co-Ce samples. Fortunately, the cathodic oxygen reduction reaction can produce a lot of OH^-, which causes an increase in pH of the surrounding region of cathode by diffusion and migration [42]. Furthermore, the dissolution rate of Ce will be accelerated by the increased pH, which leads to a shorter time to reach $C_{crit,Ce}$ and more precipitations on the surface of cathode [8]. Therefore, the effect of Ce content on the stable OCP of Al-Co-Ce amorphous alloys is associated with both the accelerated anodic reaction and the inhibited cathodic reaction with the increase in Ce content as shown in Fig. 13, and the coupling of them displays a decreased OCP with the increase in Ce content.

3.7. *Effect of Ce content on the mechanism of corrosion inhibition*

In Al-Co-Ce amorphous alloys, Ce is the major corrosion-inhibition element in 0.6 M NaCl solution. According to the XPS spectrum of Ce $3d_{5/2}$, the surface film of Al-Co-Ce alloy with 4 at.% Ce only contains Ce (0) and Ce_2O_3, whose relative contents are 38.3 at.% and 61.7 at.% respectively. But for the sample with 7 at.% Ce, the surface film contains CeO_2 in addition to Ce (0) and Ce_2O_3 with relative contents 23.6 at.%, 29.4 at.% and 47 at.% respectively. The existence of CeO_2 indicates some changes in the corrosion inhibition reactions. In general, the dissolution processes of Ce are as follows:

$$Ce \rightarrow Ce^{3+} + 3e^- \tag{6}$$

$$Ce^{3+} + 3OH^- \rightarrow Ce(OH)_{3(s)} \tag{7}$$

In an alkaline solution (pH > 7.2) containing Ce^{3+}, $Ce(OH)_{3(s)}$ is the main substance which is equivalent to the aqueous compound of Ce_2O_3 ($Ce_2O_3{\cdot}3H_2O$) and usually covers on the surface of cathode thereby hindering oxygen reduction reaction [21]. Although the pH of solution used in this research is 6.5, the pH of the surrounding region of cathode should be above 7.2 due to the production of OH^- [43]. Thus, it is easy to form $Ce(OH)_{3(s)}$, which has been confirmed by XPS. However, it is difficult to transform to the tetravalent Ce for the trivalent Ce unless in certain conditions, such as increased oxygen content or a high pH [22,24]. On the oxygen content, Fig. 11 exhibits the concentration depth profiles of oxygen for the samples with 4 at.% and 7 at.% Ce, which are immersed in 0.6 M NaCl solution for four days. It is evident that the oxide film formed on the sample with 7 at.% Ce has a higher oxygen content and greater thickness than that of the sample with 4 at.% Ce. Therefore, the increase of oxygen content should be one of the most important reasons for the formation of CeO_2 in the film. In addition, the increased local pH because of oxygen reduction reaction can also be an important reason. However, the film formed on the sample with 4 at.% Ce does not contain CeO_2 after immersion in 0.6 M NaCl solution for four days, so the effect from pH can be excluded. Regardless of the oxygen reduction reaction is either a four electron process or a two electron process, the reaction products are same, as shown by the following equations [22]:

$$4Ce^{3+} + O_2 + 4OH^- + 2H_2O \rightarrow 4Ce(OH)_2^{2+} \quad 4e- \tag{8}$$

$$2Ce^{3+} + 2OH^- + H_2O_2 \rightarrow 2Ce(OH)_2^{2+} \quad 2e- \tag{9}$$

The resulting product $Ce(OH)_2^{2+}$ will continue to react with OH^- producing CeO_2:

$$Ce(OH)_2^{2+} + 2OH^- \rightarrow CeO_2 + 2H_2O \tag{10}$$

Although Fahrenholtz et al. hold that the corrosion resistance is not related to the type of Ce oxides [44]. However, more OH^- is needed for the formation of CeO_2 compared with $Ce(OH)_{3(s)}$ or $Ce_2O_3{\cdot}3H_2O$, indicating the low generation efficiency of CeO_2. Some previous investigations also have shown that the trivalent Ce indeed has better performance in corrosion inhibition than the tetravalent Ce [45]. Therefore, it is reasonable to infer that the formation of CeO_2 is detrimental to the corrosion resistance of Al-Co-Ce amorphous alloys.

4. Conclusions

(1) The Al-Co-Ce amorphous alloy with 4 at.% Ce presented the lowest i_{pass} and N_D in 0.6 M NaCl solution indicating the best corrosion resistance, and adding excess Ce led to the reduced corrosion resistance. The passive film of Al-Co-Ce amorphous alloy with a low Ce content (4 at.%) had more protective Al (0) and Al_2O_3, while the alloy with a high Ce content (7 at.%) possessed more ($Al(OH)_3$), which is a significant reason for the decreased corrosion resistance of Al-Co-Ce alloy with the increase in Ce content.

(2) The OCP of Al-Co-Ce amorphous alloys showed a decreased tendency with the increase in Ce content, which was attributed to the accelerated anodic reaction and the inhibited cathodic reaction with the increase in Ce content.

(3) The corrosion inhibition reactions of Al-Co-Ce amorphous alloys were changed with the increase in Ce content. There existed CeO_2 in the film of the Al-Co-Ce amorphous alloy with 7 at.% Ce,

which was related to the increased oxygen content in the surface film leading to the oxidation of Ce (III) to Ce (IV). The formation of CeO_2 is detrimental to the corrosion resistance.

References

[1] Y. He, S.J. Poon, G.J. Shiflet, Science 241 (1988) 1640–1642.
[2] A.P. Tsai, A. Inoue, T. Masumoto, Metall. Trans. A 19 (1988) 1369–1371.
[3] H. Guo, C. Jiang, B. Yang, J. Wang, J. Mater. Sci. Technol. 33 (2017) 1272–1277.
[4] Y. Wu, H. Wang, X.J. Liu, X.H. Chen, X.D. Hui, Y. Zhang, Z.P. Lu, J. Mater. Sci. Technol. 30 (2014) 566–575.
[5] R.S. Maurya, T. Laha, J. Mater. Sci. Technol. 31 (2015) 1118–1124.
[6] F. Presuel-Moreno, M.A. Jakab, N. Tailleart, M. Goldman, J.R. Scully, Mater. Today 11 (2008) 14–23.
[7] M.A. Jakab, J.R. Scully, Nat. Mater. 4 (2005) 667–670.
[8] J.R. Scully, F. Presuel-Moreno, M. Goldman, R.G. Kelly, N. Tailleart, Corrosion 64 (2008) 210–229.
[9] M.A. Jakab, J.R. Scully, Corrosion 64 (2008) 198–209.
[10] Corrosion Prevention of Bridge Tendons using Flexible Filler Materials, Francisco J Presuel-Moreno, Carlos Castaneda, Ingrid Santillan, Amirkhosro Kazemi, Fujian Tang, 2018
[11] N.R. Tailleart, R. Huang, T. Aburada, D.J. Horton, J.R. Scully, Corros. Sci. 59 (2012) 238–248.
[12] A.M. Lucente, J.R. Scully, J. Electrochem. Soc. 155 (2008) C234–C243.
[13] Chloride Diffusivity and Resistivity of Cured and Mature Binary/Ternary Concrete, FJ Presuel-Moreno, S Barman, F Raof, Amirkhosro Kazemi - 2019
[14] M.E. Goldman, N. Unlu, G.J. Shiflet, J.R. Scully, Electrochem. Solid State Lett. 8 (2005) B1–B5.
[15] Corrosion Propagation of Carbon Steel Rebars in High Performance Concrete FJ Presuel-Moreno, R Bencosme, K Hoque, M Nazim,Amirkhosro Kazemi, Fujian Tang - 2018
[16] M.A. Jakab, F. Presuel-Moreno, J.R. Scully, Corrosion 61 (2005) 246–263.
[17] N.R. Tailleart, B. Gauthier, S. Eidelman, J.R. Scully, Corrosion 68 (2012).
[18] Z. Li, H. Jiang, Y. Wang, D. Zhang, D. Yan, L. Rong, J. Mater. Sci. Technol. 34
[20] Z. Zheng, J. Wang, Q. Xing, Z. Sun, Y. Wang, J. Non-Cryst. Solids 379 (2013) 54–59.
[21] F.J. Presuel-Moreno, M.A. Jakab, J.R. Scully, J. Electrochem. Soc. 152 (2005) B376–B387.
[22] A.J. Aldykiewicz, A.J. Davenport, H.S. Isaacs, J. Electrochem. Soc. 143 (1996) 147–154.
[23] A.J. Davenport, H.S. Isaacs, M.W. Kendig, Corros. Sci. 32 (1991) 653–663.
[24] A.J. Aldykiewicz, H.S. Isaacs, A.J. Davenport, J. Electrochem. Soc. 142 (1995) 3342–3350.
[25] M. Mouanga, F. Andreatta, M.E. Druart, E. Marin, L. Fedrizzi, M.G. Olivier, Corros. Sci. 90 (2015) 491–502.
[26] F. Andreatta, M.E. Druart, E. Marin, D. Cossement, M.G. Olivier, L. Fedrizzi, Corros. Sci. 86 (2014) 189–201.
[27] W. Xiong, G.T. Qi, X.P. Guo, Z.L. Lu, Corros. Sci. 53 (2011) 1298–1303.
[28] R.C. Zeng, Y. Hu, F. Zhang, Y.D. Huang, Z.L. Wang, S.Q. Li, E.H. Han, Trans. Nonferrous Metals Soc. China 26 (2016) 472–483.
[29] Y. Wang, S.L. Jiang, Y.G. Zheng, W. Ke, W.H. Sun, J.Q. Wang, Surf. Coat. Tech. 206 (2011) 1307–1318.
[30] R.Z. Zand, K. Verbeken, A. Adriaens, Int. J. Electrochem. Soc. 8 (2013) 548–563.
[31] C.Q. Fu, F. Yong, Q.L. Zhang, Mater. Mach. Dev. Technol. Ind. Prod. (2014) 247–251.
[32] J.C.S. Fernandes, R. Picciochi, M. Da Cunha Beloa, T.M. Silva, M.G.S. Ferreira, I.T.E. Fonseca, Electrochim. Acta 49 (2004) 4701–4707.
[33] K.L. Levine, D.E. Tallman, G.R. Bierwagen, J. Mater. Process. Technol. 199 (2008) 321–326.
[34] Y. Liu, G.Z. Meng, Y.F. Cheng, Electrochim. Acta 54 (2009) 4155–4163.
[35] E.E. Coral-Escobar, M.A. Pech-Canul, M.I. Pech-Canul, J. Solid State Electrochem. 14 (2010) 803–810.
[36] Y. Liu, Y.F. Cheng, J. Appl. Electrochem. 41 (2011) 151–159.
[37] J.L. Lv, H.Y. Luo, J.P. Xie, Appl. Surf. Sci. 273 (2013) 192–198.
[38] E. Stoyanova, D. Nikolova, D. Stoychev, P. Stefanov, T. Marinova, Corros. Sci. 48 (2006) 4037–4052.
[39] Z.M. Wang, J. Zhang, X.C. Chang, W.L. Hou, J.Q. Wang, Intermetallics 16 (2008) 1036–1039.
[40] M.A. Arenas, M. Bethencourt, F.J. Botana, J. de Damborenea, M. Marcos, Corros. Sci. 43 (2001) 157–170.
[41] M.A. Arenas, J.J. de Damborenea, Electrochim. Acta 48 (2003) 3693–3698.
[42] J.B. Han, B.N. Brown, D. Young, S. Nesic, J. Appl. Electrochem. 40 (2010) 683–690.
[43] J. Han, B.N. Brown, D. Young, S. Nešić, J. Appl. Electrochem. 40 (2010) 683–690.
[44] W.G. Fahrenholtz, M.J. O'Keefe, H.F. Zhou, J.T. Grant, Surf. Coat. Technol. 155 (2002) 208–213.
[45] E.A. Matter, S. Kozhukharov, M. Machkova, V. Kozhukharov, Corros. Sci. 62 (2012) 22–33.